JOURNAL OF GEOPHYSICAL RESEARCH, VOL. 102, NO. E6, PAGES 13,321–13,340, JUNE 25, 1997

Crater morphometry and modification in the Sinus Sabaeus and Margaritifer Sinus regions of Mars

Robert A. Craddock[1] and Ted A. Maxwell
Center for Earth and Planetary Studies, National Air and Space Museum, Smithsonian Institution, Washington, D. C.

Alan D. Howard
Department of Environmental Sciences, University of Virginia, Charlottesville

Abstract. Degraded craters in the southern highlands are indicative of an early martian climate much different than the present. Using a photoclinometric model, analyses of degraded crater morphometry have revealed the stages of crater modification and, for the first time, allow a quantitative assessment of the amount of material eroded in the highlands. Central peaks of fresh craters are removed early by degradational processes. The sharp rims of fresh craters also become rounded while the interior slopes become shallower. Continued degradation causes the crater rim to lower, and infilling produces a broad, flat crater floor. Contrary to earlier observations, the degree of rim modification does not appear to be dependent on the presence of ancient valley networks. During degradation, the diameter of the impact craters also increases due to backwasting. A simple algebraic model balancing the measured amount of infilling with that eroded from the interior slopes suggests that the crater diameters were enlarged by 7 to 10% initially, agreeing with prior observations. These models suggest that larger diameter (i.e., 50 km) craters were enlarged a greater amount than smaller diameter craters, which is opposite to what should be observed. To explain this discrepancy, a ~10 m thick deposit, presumably aeolian in origin, must have been emplaced within the crater interiors following cessation of the degradational process. By the terminal stage of degradation, crater diameters appear to have been enlarged by 30%. In addition, a deposit ~60 m average thickness must have been emplaced within these rimless craters to explain the discrepancy in crater enlargement. Because this deposit is contained only within the highly eroded, rimless craters, this material most likely originated from erosion of the surrounding terrain. The measured crater morphometry has allowed us to develop equations describing the amount of material eroded at any given stage of degradation. Applying these equations to craters within the Margaritifer Sinus and Sinus Sabaeus region indicates that an equivalent of ~200 m of highland material was eroded and redistributed within the study area. Depending upon model chronology, degradation operated for either 400 or 600 million years, suggesting that erosion rates were on the order of ~0.0003 to 0.0005 mm/yr. These erosion rates are equivalent to those determined for terrestrial periglacial environments. Two-dimensional simulations of some possible degradational processes suggest that fluvial erosion and deposition combined with diffusional creep come closest to producing equivalent degrees of modification through the range of crater diameters investigated in this study (20 to 50 km). However, these processes are inefficient at producing the amount of crater enlargement observed, suggesting that crater interior slopes may have also been undermined by sapping. These results imply that geologic processes related to precipitation dominated the early martian environment. Our working hypothesis is that this precipitation was due to the presence of a primordial atmosphere which condensed and collapsed (i.e., precipitated) into the martian regolith; a process which ceased during the late Hesperian/early Amazonian (3.5 to 1.8 Ga).

Introduction

One of the long-standing mysteries in the exploration of Mars by spacecraft is the mechanism responsible for modifying many of the impact craters seen in the southern cratered highlands. Mariner 4 data first revealed that martian craters are morphologically more Earth-like than lunar-like. *Leighton et al.* [1965] observed martian craters of widely different degrees of preservation and, it was presumed, ages. Successive Mariner flights provided additional data, and because of the predominance of present-day aeolian activity it was first suggested that loose crater ejecta had been removed and redistributed to explain the modified appearance of the martian craters [*Hartmann*, 1971; *Chapman*, 1974]. Alternatively, *Jones* [1974] and *Chapman and*

[1]Also at Department of Environmental Sciences, University of Virginia, Charlottesville.

Paper number 97JE01084.
0148-0227/97/97JE-01084$09.00

Jones [1977] suggested that water acted as a major erosive agent during an early martian crater obliteration event. Volcanism is another potential process suggested for crater modification [*Arvidson et al.*, 1980]. Because the geologic materials that contain degraded impact craters are the oldest exposed units on the planet [*Scott and Tanaka*, 1986; *Greeley and Guest*, 1987], these hypotheses obviously imply very different geologic histories for early Mars.

Martian highland crater morphology has been the subject of renewed interest in recent years, primarily because it does contain clues about the early martian environment. Aeolian mechanisms involving deep deposits of material are still strongly advocated [*Wilhelms and Baldwin*, 1989; *Moore*, 1990; *Grant and Schultz*, 1990, 1991a,b]. However, only a process or a combination of processes involving fluvial erosion can explain the size range of affected craters, the range in morphology, the timing of degradation, and the amount of erosion that must have taken place [*Craddock and Maxwell*, 1990, 1993; *Grant and Schultz*, 1994; *Barlow*, 1995]. Did early Mars have dust storms that were orders of magnitude more intense than those seen today? Or did an early atmosphere condense and erode the martian highlands as the water settled into the regolith? The answer has importance for understanding the martian atmospheric and climatic history, the history of water and aeolian material on Mars, the nature of the highland units, and in assessing the likelihood that life has developed on Mars.

Previously, we examined modified craters in the Amenthes and Tyrrhena regions of Mars [*Craddock and Maxwell*, 1990]. The evidence from this area suggests that an erosional process combined with sediment redeposition, as opposed to a purely depositional process such as emplacement of airfall or volcanic materials, is capable of explaining the observed morphology and size range of degraded craters. Iterative fits of the measured crater populations to model size-frequency distribution curves, which accounted for both modification of larger craters and eradication of small diameter craters, suggested that between 0.5 to 1.5 km of highland material was removed and redistributed. A more complete examination of the highland crater population between ±30° latitude [*Craddock and Maxwell*, 1993] identified craters preserved in various stages of modification. Based on superposed fresh crater populations, it also appears that modification ceased at higher elevations (e.g., 3-4 km, Late Noachian) before it did at lower elevations (e.g., 1-2 km, Early Hesperian). This was interpreted to indicate that cessation of fluvial activity was coupled to desiccation of a volatile reservoir with time or possibly that decreases in martian atmospheric pressures caused cloud condensation, and thus rainfall, to occur at progressively lower elevations [*Craddock and Maxwell*, 1993].

In this study we focus on the morphometry of both degraded and fresh craters derived through photoclinometric measurements. These measurements allow us to quantify the amounts of erosion and/or deposition that have occurred in the highlands, observe and quantify changes in crater morphology through advanced stages of modification, and identify the possible process(es) responsible for highland crater modification. Due to its proximity to the southern Chryse Planitia outflow channel complex, the possibility that the region may have contained ancient aqueous basins [*Goldspiel and Squyres*, 1991], the numerous ancient valley networks contained on highland materials [e.g., *Carr and Clow*, 1981], and the variety of geologic processes suggested by analyses of crater populations in the local highlands and surrounding plains [*Maxwell and Craddock*, 1995], we have initiated our analyses in the Sinus Sabaeus and Margaritifer Sinus regions between -14° to -31° latitude and 337° to 23° longitude (Figure 1). At these latitudes, influences on crater morphology from variations in the amount of volatiles within the substrate [*Barlow and Bradley*, 1990], increasing thickness of possible aeolian deposits with higher latitudes [*Soderblom et al.*, 1973; *Arvidson et al.*, 1976; *Mouginis-Mark*, 1979], and modification due to terrain softening [*Squyres and Carr*, 1986; *Jankowski and Squyres*, 1992] can be avoided. The surface area represented by these materials is ~1.1 x 10^6 km^2, or ~0.8% of the surface area of the planet. Because it appears that crater morphometry is dependent upon geologic unit [*Barlow*, 1992, 1993] and that other highland materials may contain deposits that were emplaced by later-stage, local processes, we have constrained our initial analysis to the dissected materials (Npld) identified by *Scott and Tanaka* [1986] and *Greeley and Guest* [1987]. These materials are the most widespread geologic unit on Mars and represent some of the oldest exposed materials on the surface.

We measured the morphometry of 264 fresh impact craters and 186 degraded craters ~3 to 76 km in diameter using the photoclinometric algorithm written for the Planetary Image Cartography System or PICS [*Davis and Soderblom*, 1984] (see appendix). The images were radiometrically calibrated, red and clear filter Viking Orbiter data (frame numbers 084A17, 579A30, 32, 39, 51, 53, 55, 60, 581A50, 52, 55, 615A43-45, 47, 48, 50, 51, 71-73, and 618A41-42) with resolutions of ~200 m/pixel and phase angles of ~75° to 95°. The derived photoclinometric profiles were compared to morphologic classes assigned to degraded craters in earlier work [*Craddock and Maxwell*, 1993], and geometric relations describing these crater shapes (e.g., depth as a function of diameter) were determined. These geometric relations were used to evaluate the extent of crater modification at a variety of crater diameters (20, 30, 40, and 50 km) and determine the scale dependency of the modification process(es). These results were then compared to a two-dimensional computer model [*Howard*, 1994] that simulated effects of fluvial erosion and mass wasting on fresh craters. Results from this investigation suggest that both fluvial, diffusive, and, to a limited extent, aeolian processes have played roles in modifying the cratered highlands of Mars. In addition, it appears that seepage of groundwater from the base of the crater interior may be necessary to not only help remove the rims of larger diameter craters but also to explain the amount of crater enlargement that has apparently occurred at all crater diameters. These results indicate that early Mars experienced wide-spread precipitation, fluvial processes, and groundwater flow, and imply that the early martian climate and geologic processes may have been similar to those occurring today in terrestrial periglacial environments.

Crater Morphometry

Fresh Craters

Pike and Davis [1984] measured the morphometry of 74 fresh complex craters with diameters >3 km on Mars using the *Davis*

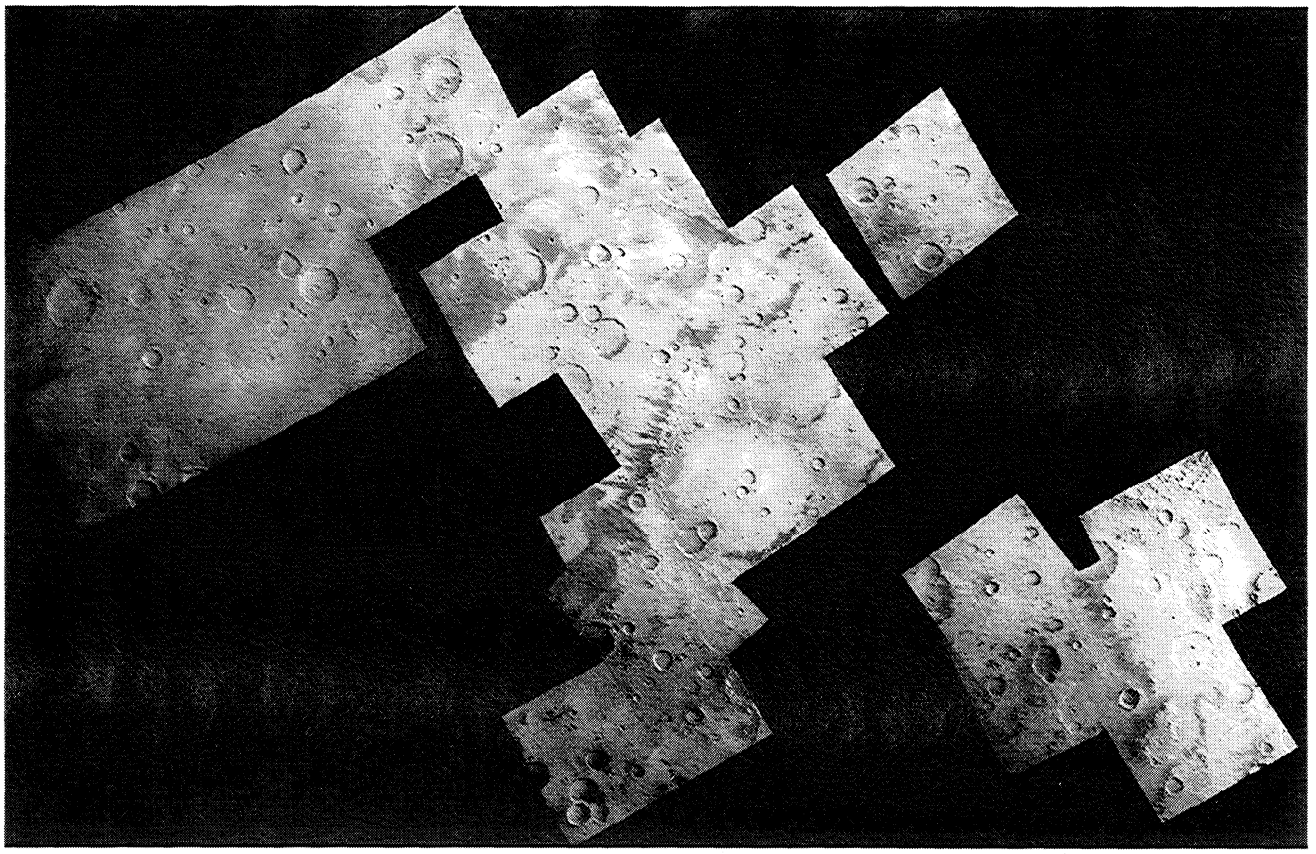

Figure 1. Photomosaic of the Sinus Sabaeus and Margaritifer Sinus study area. The gaps in image coverage represent the occurrence of Nplr and other materials mapped by *Greeley and Guest* [1987] that were not included in the analysis.

and Soderblom [1984] photoclinometric model (see appendix). The morphometric relations derived by these investigators were used in numerous studies [*DeHon*, 1985; *Craddock and Maxwell*, 1990, 1993; *Barlow*, 1992, 1995; and many others]. However, because impact crater morphometry appears to vary by location [*Barlow*, 1992, 1993], our measurements of fresh impact craters were restricted to the Margaritifer Sinus region for accurate determination of the pre-degradation crater morphometry.

Fresh impact craters have obvious ejecta blankets, sharply defined rims, frequently contain small central peaks, and are superposed on all ancient valley networks and degraded craters (Figure 2a). Fresh craters with both lunar-like and "fluidized" ejecta were observed in the study area; however, these differences were not distinguished in the analysis. This is due in part to the infrequent occurrence of lunar-like craters, but also because it is not possible to determine the initial (i.e., fresh) morphology of a degraded crater. It is also important to note that the population of fresh impact craters postdates the period of highland degradation, and the physical characteristics of the highland materials may have changed during degradation. Thus, the morphology of fresh impact craters may have changed through time, but it is not possible to determine this. For comparison with other geologic units and the martian time stratigraphic boundaries [*Tanaka*, 1986], we normalized the cumulative number of craters >5 km in diameter to 10^6 km^2. In a separate study [*Maxwell and Craddock*, 1995], we observed that degradation in the highlands of Margaritifer Sinus ceased at an N[5] age of 217, or the late Noachian (~3.5-3.8 Ga) based on crater density boundaries determined by *Tanaka* [1986].

The 264 fresh craters measured range in size between 2 and 43 km in diameter. We have measured ~4 times more craters than *Pike and Davis* [1984] did in their initial analysis, and our measured morphometric relations (Figure 3) support their observations. The relationships of primary importance are crater depth and rim height versus crater diameter. The least-squares regression fit for crater depth versus diameter uses logarithmic transformation and is described by the equation

$$d_F = 0.189\ (\pm 0.035) D_F^{0.675\ (\pm 0.041)} \qquad r = 0.72 \qquad (1)$$

where d_F is the fresh crater depth (km) measured from the lowest point in the crater to the maximum rim height and D_F is the fresh crater diameter (km) defined by the occurrence of maximum rim height. For comparison, *Pike and Davis* [1984] found values of 0.309±0.049 for the coefficient and 0.504±0.061 for the exponent. The correlation coefficient for equation (1) is less than the value for complex craters obtained by *Pike and Davis* [1984] ($r = 0.87$).

For crater rim height, the least-squares fit is described by

$$h_F = 0.066\ (\pm 0.064)\ D_F^{0.497\ (\pm 0.076)} \qquad r = 0.38 \qquad (2)$$

where h_F is the fresh crater rim height in kilometers measured from the maximum rim height to the precrater ground level. The

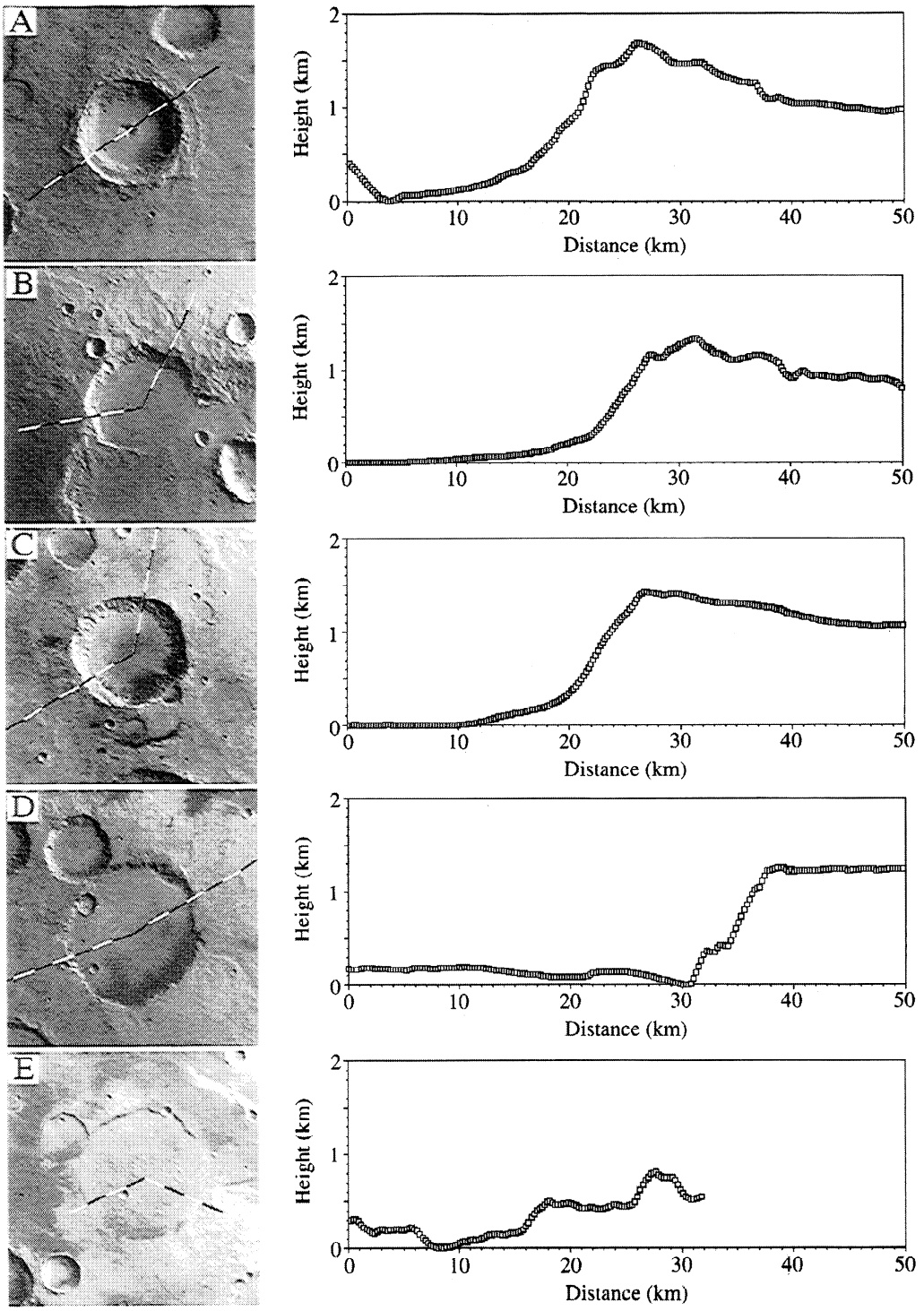

Figure 2. Examples of the crater types classified within the martian highlands and their corresponding photoclinometric profiles. Craters range in diameter between ~25 and 40 km. (a) Fresh impact crater. Note the sharply defined rim and central peak. (b) Type B degraded crater containing numerous ancient networks on the ejecta blanket. Note the absence of a central peak. (c) Type C degraded crater. Although in plan view this crater appears to be rimless (Viking orbiter frame 579A59), a rounded rim crest is still present. Central peak has been eroded to a flat floor. Morphometric similarities between Type B and C craters compelled us to classify these crater types together. (d) Type D degraded impact crater. At this stage of degradation, only a small portion of the rim remains. The uneven floor is most likely the result bright, interior deposits. Such a crater was not included in the study, but is shown for illustrative purposes. (e) Type E degraded crater containing what *Goldspiel and Squyres* [1991] suggested as being sedimentary fill which produces an irregular crater floor. A crater rim is absent and the crater appears to have been breached in places. The irregular albedo pattern around this crater also precludes including it in our data analyses.

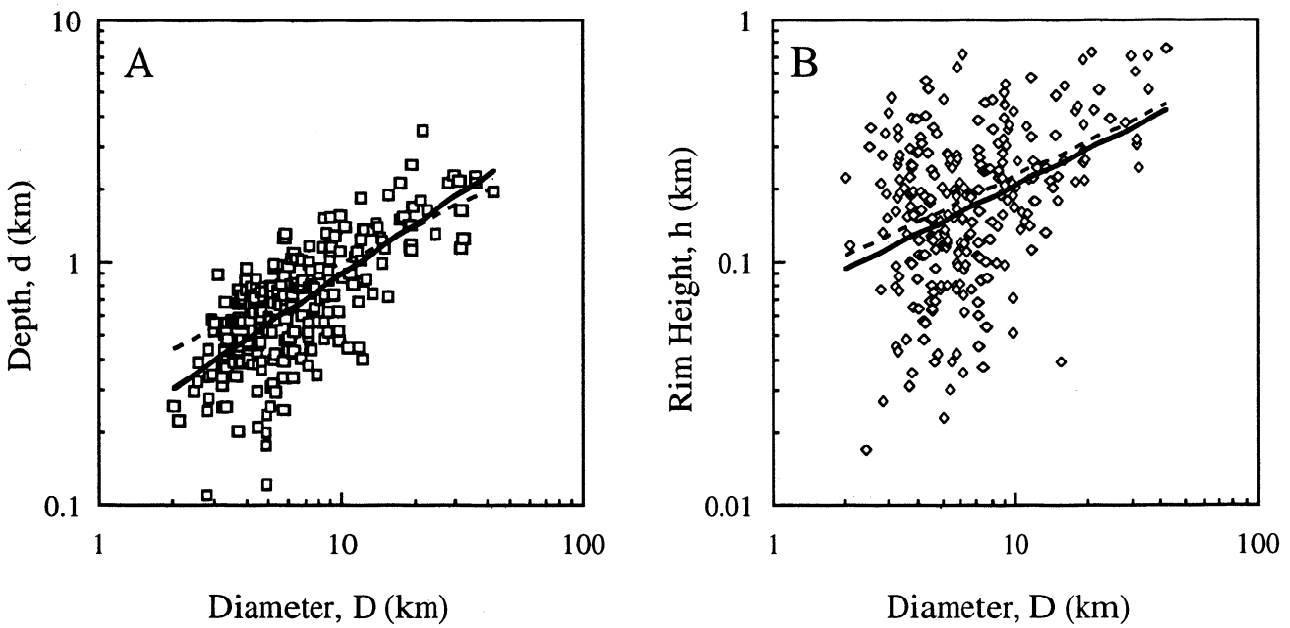

Figure 3. (a) Fresh crater depth versus diameter. (b) Fresh crater rim height versus diameter. *Pike and Davis'* [1984] observed relationships (dashed lines) are included for comparison.

low correlation coefficient associated with this relation suggests that fresh crater rim height is highly variable, probably due to the overall rugged nature of the martian highlands which makes it difficult to determine the precrater datum. It is important to note again that both equations (1) and (2) describe both simple and complex craters, and the variability of these craters geometry [*Craddock and Chuang,* 1996] may have also reduced the correlation.

Figure 4 shows typical fresh crater profiles obtained from photoclinometric measurements. Craters shown are representative of each morphologic class at 10-km-diameter intervals. The bowl-shape of the fresh crater interiors are apparent as well as the sharp rim crests. The ejecta of fresh, lunar-like craters grades slowly into the surrounding plains and the fluidized ejecta termination was often visible as an abrupt change in elevation. The topographic expression of the continuous ejecta for both types of fresh craters is recognizable out to an average of 1.18 ± 0.03 crater diameters. Because this relation is based on the derived photoclinometric profiles, it makes no effort to account for the irregular, lobate occurrence of fluidized ejecta craters.

Degraded Craters

The most noticeable morphologic attributes of degraded impact craters in the martian highlands are their flat-floors and the apparent lack of a crater rim. From Mariner spacecraft data *McGill and Wise* [1972] and *Arvidson* [1974b] showed that these craters underwent progressive stages of degradation. After analyses of Viking orbiter images, *Craddock and Maxwell* [1993] proposed a five-stage degradation sequence that begins with an unmodified fresh crater (Figure 2a). During the initial stage of degradation (Figure 2b), fresh craters quickly lost central peaks, and ejecta blankets also became incised by well-developed ancient valley networks. Although the drainage density of such valley networks has not been studied specifically on a large sample size, *Grant and Schultz* [1994] suggested that comparable network densities on the crater Millochau (21.5°S, 274°W) reflect incisement by surface runoff. As degradation proceeded, ejecta was removed and the rims lowered to the point where slope angles no longer support valley incisement (Figure 2c). Eventually the rims were removed completely and material eroded from the surrounding highlands may have been transported into the crater interior (Figure 2d). Finally, in advanced stages of degradation, the craters walls were often breached and, in instances, the craters became deeply buried (Figure 2e). From their analysis of terrestrial impact craters, *Grant and Schultz* [1993] suggested that martian craters may have been enlarged by <10% due to backwasting that occurred during degradation.

To categorize the degraded craters and to test whether our prior classes can be distinguished topographically, we retained the degraded crater classification defined by *Craddock and Maxwell* [1993]. The degraded crater type designation refers to the letter subscript used in Figure 2 (i.e., a Type B crater is pictured in Figure 2b, etc.). The units for all equations given below (i.e., equations (3) through (9)) are kilometers. The relationships describing crater rim height versus diameter for Type B and Type C craters are described by the equations

$$h_B = 0.010\ (\pm 0.006)\ D_B^{0.882\ (\pm 0.301)} \qquad r = 0.53 \qquad (3a)$$

$$h_C = 0.024\ (\pm 0.011)\ D_C^{0.656\ (\pm 0.327)} \qquad r = 0.38 \qquad (3b)$$

where h_B and h_C are the crater rim heights of degraded Type B and C craters, respectively, and D_B and D_C are their diameters. Their associated depths are described by

$$d_B = 0.106\ (\pm 0.051)\ D_B^{0.670\ (\pm 0.221)} \qquad r = 0.54 \qquad (4a)$$

$$d_C = 0.034\ (\pm 0.017)\ D_C^{1.024\ (\pm 0.351)} \qquad r = 0.47 \qquad (4b)$$

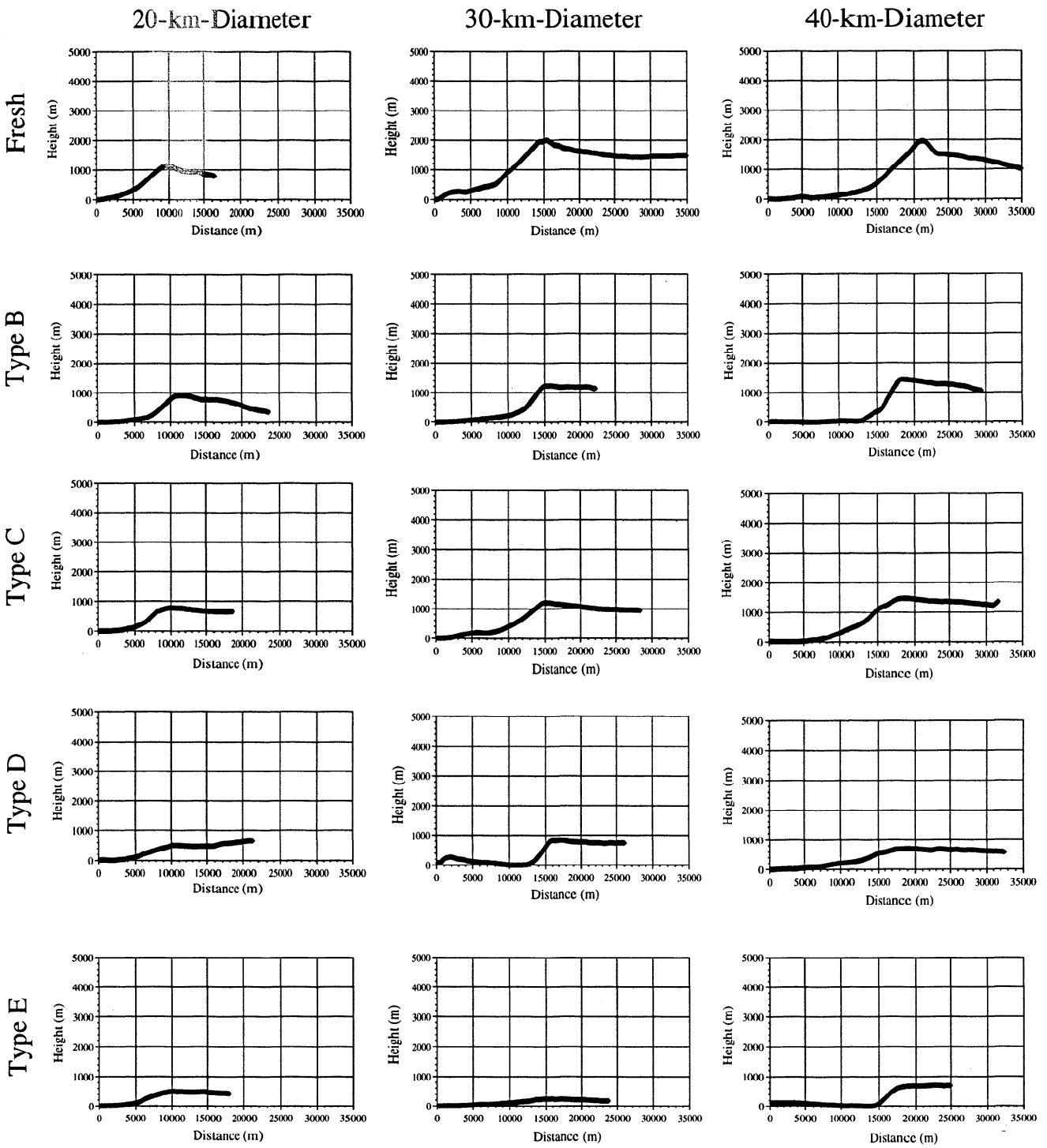

Figure 4. Topographic profiles of typical craters in various stages of degradation sampled in this study derived from photoclinometry. Because the Type D crater rims are typically less than a few hundred meters high, they are not easily seen at the scale of these figures.

where d_B and d_C are the depths of degraded Type B and C craters, respectively. Figure 5 shows the similarity between these corresponding functions (equations (4a) and (4b)), supporting the visual observations made from the actual profiles. Because both classes of craters are indistinguishable based on topography, Type B and C craters were grouped together to form the equations

$$h_{B/C} = 0.016\ (\pm 0.008)\ D_{B/C}^{0.764\ (\pm 0.213)} \quad r = 0.44 \qquad (5)$$

$$d_{B/C} = 0.072\ (\pm 0.038)\ D_{B/C}^{0.792\ (\pm 0.194)} \quad r = 0.49 \qquad (6)$$

Type D craters have only a small amount of rim material remaining. The rim height is described by

$$h_D = 0.001\ (\pm 0.000)\ D_D^{1.161\ (\pm 0.257)} \quad r = 0.54 \qquad (7)$$

where h_D is the crater rim height and D_D is the corresponding diameter. Type D craters also have broad, flat floors and shallow

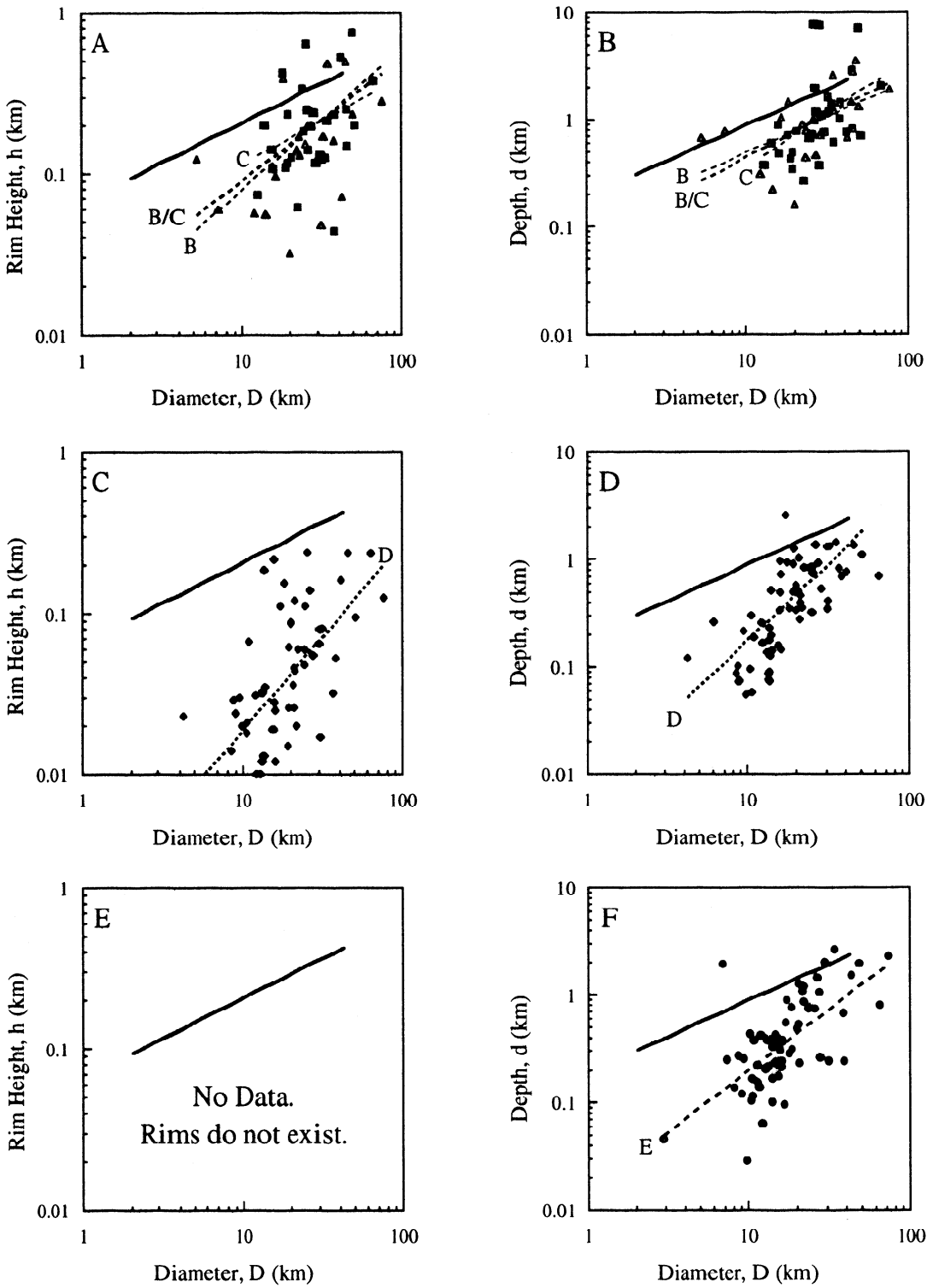

Figure 5. Morphometric relations of degraded impact craters. Fresh crater relationships (solid lines) are shown for comparison. (a) Type B, Type C, and Type B/C combined crater rim height versus diameter. (b) Type B, Type C, and Type B/C combined crater depth versus diameter. (c) Type D crater rim height versus diameter. (d) Type D crater depth versus diameter. (e) By definition, Type E craters have no observable crater rim. Note, however, that the crater rim height decreases with increased degradation in the other crater types. (f) Type E crater depth height versus diameter.

interior slopes (Figure 4). At any given diameter, the depth of a Type D crater is also noticeably shallower than its less degraded counterpart. The depth of Type D craters is given by the expression

$$d_D = 0.006\ (\pm 0.003)\ D_D^{1.422\ (\pm 0.220)} \quad r = 0.63 \qquad (8)$$

The primary morphologic difference separating the Type D crater from the Type E is the presence of a remnant crater rim. Type E craters have no crater rims and are distinguished from the surrounding highlands by a broad, flat floor and shallow interior slope. They are described by the equation

$$d_E = 0.015\ (\pm 0.008)\ D_E^{1.119\ (\pm 0.167)} \quad r = 0.65 \qquad (9)$$

Other morphometric relationships that were determined for both fresh and degraded craters include the depth below the precrater datum (d_{pc}), the diameter of the crater at precrater ground height (D_{pc}), and the floor diameter (D_f). These data are presented in Table 1.

Observations

These photoclinometric measurements provide the first detailed topographic information about the crater classifications. Representative profiles of each crater class are presented in Figure 4. Although the plan view classification provides a logical way of separating the degradation state of craters, two of the original classes of *Craddock and Maxwell* [1993] cannot be distinguished on the basis of topography. Morphologically, the only difference between Type B and Type C craters is seen in plan view (Figures 2b and 2c) with Type B crater ejecta blankets containing more ancient valley networks than Type C craters. In our prior work, it was also noted that Type C craters contained fewer ancient valley networks on the ejecta blanket, which was interpreted to mean that the exterior slope had been eroded to a point where it was no longer possible for incisement to occur. However, it is apparent from the topographic profiles that both Type B and Type C craters generally appear similar (Figures 2 and 4). The most noticeable difference between these craters and their fresh counterparts is that the interiors are no longer bowl-shaped. Instead, the interior has a broad floor that is flat to gently sloping in relief, which is most likely due to backwasting and infilling. The crater rim is also more rounded, reflecting erosion and slumping into the interior. Subsequent aggradation or post-degradation modification may have buried or obscured valley networks on some craters.

With continued degradation, the Type D craters take on a "cookie cutter" morphology (Figure 2d). However, photoclinometric measurements reveal the faint presence of a rim, and interior slopes have also typically become shallower (Figure 4). At the final stage of crater degradation (Type E craters), infilling appears to become an important process because the depth of craters becomes shallower. Without the topographic barrier from the crater rim, materials eroded from the surrounding craters and highlands could be transported across the surface and into Type E crater depressions.

Crater Degradation

As degradation progressed, the crater rims were lowered and became rounded, and the diameter of the crater increased due to backwasting. These complicated processes interacting together make evaluating the patterns of erosion and deposition difficult to determine. For example, a 20-km-diameter fresh crater does not evolve into a 20-km degraded crater, so the resulting change in depth from rim erosion and infilling is not easily calculated from the derived morphometric relations. Either a certain amount of rim downcutting or a certain amount of enlargement from backwasting must be assumed before the other can be approximated. In order to determine the amount of crater infilling that occurred solely as a result of backwasting of the rim, we begin by modeling the shape of a fresh crater using the derived morphometric relationships (equations (1) and (2), Table 1), and balance the material amounts estimated from rim backwasting and crater infilling.

As a first-order approximation, crater morphometry was modeled algebraically. Appropriate crater depths and rim heights were calculated from the measured relations presented above and in Table 1. Average interior slopes for degraded craters at various stages were taken to be the average angle from the rim crest to the edge of the crater's flat floor, which was operationally defined as the point along the profile where elevational differences between adjacent measurements were less than ~10 m. Average interior slope for fresh craters was taken to be the average angle from the rim crest to the diameter of the crater at the precrater ground height. This more subjective interior angle was used because the fresh craters frequently had no discernible floor, and it would ensure that the steepest part of the interior slope would be used. The resulting average interior angles were determined to be 13.3° (± 0.3°) for the fresh impact craters, 9.5° (± 0.5°) for Type B/C craters, 7.8° (± 3.6°) for Type D, and 6.4° (±0.4) for Type E. Such angles only approximate the true interior shape of a crater, especially those of fresh craters and craters in the earliest stages of degradation, but they do describe the average crater population.

The shape of fresh craters with diameters of 20, 30, 40, and 50 km were determined. To estimate the amount of backwasting that took place during degradation, these fresh craters were compared to those of typical Type B/C craters at slightly larger diameters. The estimate of <10% enlargement due to backwasting made by *Grant and Schultz* [1993] was used as an initial constraint. Eroded and infilled crater volumes were estimated by determining the corresponding cross-sectional area (Figure 6), determining the centroids of both the eroded area and the infilled area, and then using the Theorem of Pappus, or

$$V = (2\pi b)(\text{Area}) \qquad (10)$$

where b is the radius of the centroid. The baseline for determining the difference between the two crater profiles was the precrater ground height in kilometers (i.e., the total depth of the crater, d_x, minus the crater rim height, h_x). A fresh crater was then compared to a 10% larger diameter Type B/C crater to account for backwasting. The degraded crater diameter was then adjusted until the volume of material eroded through backwasting was equal to the volume of material deposited in the crater

Table 1. Comparison of Least Squares Fits for Complex Fresh and Degraded Crater Dimensions

Crater Type	Variables (x/y)[a]	n	r	Slope	Y at X=1.0
Fresh	D/h	264	0.38	0.497 ± 0.076	0.066 ± 0.064
Type B/C	D/h	54	0.44	0.764 ± 0.213	0.016 ± 0.008
Type D	D/h	67	0.54	1.161 ± 0.237	0.001 ± 0.000
Type E	D/h	0	N/A		
Fresh	D/d	264	0.72	0.675 ± 0.041	0.189 ± 0.035
Type B/C	D/d	54	0.49	0.792 ± 0.194	0.072 ± 0.038
Type D	D/d	67	0.63	1.453 ± 0.220	0.006 ± 0.003
Type E	D/d	63	0.65	1.119 ± 0.167	0.015 ± 0.008
Fresh	D/dpc	264	0.67	0.863 ± 0.059	0.088 ± 0.050
Type B/C	D/dpc	54	0.49	0.863 ± 0.220	0.071 ± 0.043
Type D	D/dpc	67	0.62	1.507 ± 0.235	0.005 ± 0.002
Type E	D/dpc	63	0.64	1.129 ± 0.177	0.014 ± 0.006
Fresh	D/Dpc	259	0.78	1.346 ± 0.068	0.352 ± 0.058
Type B/C	D/Dpc	54	0.95	1.010 ± 0.044	0.844 ± 0.124
Type D	D/Dpc	67	0.94	0.967 ± 0.043	1.033 ± 0.143
Type E	D/Dpc	0	N/A		
Fresh	D/Df	95	0.04	0.050 ± 0.130	0.285 ± 0.114
Type B/C	D/Df	52	0.58	1.102 ± 0.180	0.261 ± 0.165
Type D	D/Df	66	0.57	0.824 ± 0.155	0.648 ± 0.237
Type E	D/Df	63	0.80	1.139 ± 0.109	0.285 ± 0.058

[a]Defined in text.

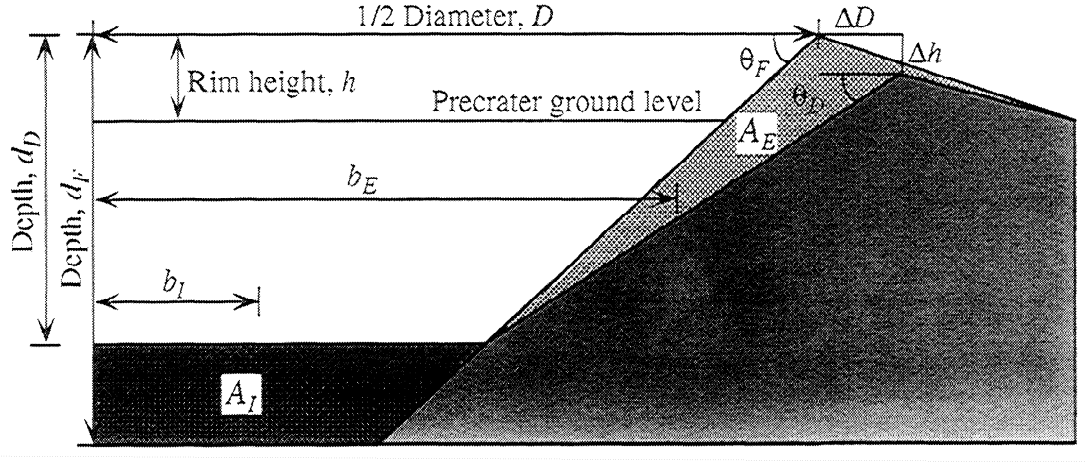

Figure 6. Schematic diagram illustrating measurements used to calculate modification in crater morphometry. Example shown is a 20-km-diameter fresh crater (4x vertical exaggeration) compared to a Type B/C degraded counterpart. Using the Theorem of Pappus (equation (10)), the volume of material eroded off crater walls was calculated by determining the area eroded (A_E) and the radius of this centroid (b_E). In an identical fashion, the volume of infilled material (represented by A_I and b_I) was also determined. Degraded crater diameters were increased ($D + \Delta D$) while maintaining a fixed θ_f and θ_d and adjusting both the rim height (Δh) and degraded crater depth (d_D) until the volumes of eroded and infilled materials balanced. In this Type B/C crater example, ΔD represents an ~6% increase in the crater diameter.

Table 2. Calculated Crater Diameter Enlargement Due to Backwasting

Fresh Crater Diameter, km	Type B/C, %	Type D, %	Type E, %
20	6.18	11.4	15.4
30	8.22	15.0	20.2
40	8.39	18.3	26.5
50	8.91	21.0	31.0

interior. After determining the approximate amount of enlargement for Type B/C craters, this process was iteratively repeated for each subsequent stage of crater degradation (Table 2).

It is important to note that the change in crater depth is not solely a result of infilling. Although the crater becomes shallower during infilling, backwasting also cuts into the highest portion of the crater rim, thus lowering it. Using the derived morphometric relationships to calculate the depth (d_x) and rim heights (h_x) of degraded craters enlarged through backwasting, it is found that during degradation the crater does not become shallower so much as the exterior (i.e., crater rim) is lowered. Table 3 shows that most of the decrease in overall crater depth is due to rim erosion. The tacit assumption made was that the surrounding terrain did not change in elevation during the degradational process.

Evidence for Aggradation

Balancing the eroded and infilled volumes allows us to estimate the amount of enlargement that takes place at various stages of degradation for different crater size classes (Table 2). For example, at the Type B/C stage of degradation, 20-km-diameter craters are enlarged by ~6%, while larger diameter craters are enlarged by increasing amounts up to ~9%. Assuming that the interior slope is constant regardless of crater diameter (found to be true), erosion should occur more rapidly for a larger diameter crater because of the larger contributing area [*Howard*, 1994]. Thus the relative amount of crater enlargement due to backwasting should be equal at any crater diameter, and all Type B/C craters should be enlarged by an equal percentage. As shown above, such a consistent relation does not hold for the size range of craters studied.

Table 3. Changes in Crater Depths Due to Rim Height Erosion

Crater Diameter, km	Fresh Depth, km	Type B/C Depth, km	% Δ Depth Due to Rim Erosion	Type E Depth, km	% Δ Depth Due to Rim Erosion
		Fresh Craters			
10	0.894	--	--	--	--
20	1.428	--	--	--	--
30	1.877	--	--	--	--
40	2.280	--	--	--	--
50	2.650	--	--	--	--
		Degraded Craters Enlarged 5% From Backwasting			
10.5	--	0.464	68	0.208	46
21	--	0.803	71	0.453	51
31.5	--	1.107	72	0.712	56
42	--	1.390	73	0.983	60
52.5	--	1.658	74	1.262	63
		Degraded Craters Enlarged 10% From Backwasting			
11	--	0.481	68	0.219	46
22	--	0.833	71	0.477	52
33	--	1.148	72	0.750	56
44	--	1.442	74	1.035	60
55	--	1.721	75	1.329	64

The observed increase in enlargement with increasing crater size can be explained by considering the measurements on which the model is based. The only processes accounted for in the measured depth changes are downcutting of the rim and infilling of the crater by backwasting. However, *Craddock and Maxwell* [1993] showed that these processes ceased at least ~3.5 Ga according to the *Hartmann et al.* [1981] crater chronology model [*Tanaka*, 1986] and since that time, aeolian processes dominated. In addition, some material ejecta from the continuing formation of impact craters may have also been deposited into the older, degraded craters. If a layer ~5 to 10 meters thick is subtracted from the floor fill estimates, then the Type B/C degraded impact craters appear to have been enlarged by ~9% at all diameters.

This result is simply a function of proportionality. The volume of a 5-10 m thick deposit is proportionally more to a 20-km-diameter crater than it is to a 50-km-diameter crater by the relationship $\pi r^2 h$, where πr^2 describes the surface area of the crater interior (assumed to be a circle) and h is the thickness of the deposit. This assumes that no volume expansion occurred for the infilled material, and eroded materials may increase in volume by as much as 50% [*Oliver*, 1979]. Alternatively, material eroded from the crater walls may have expanded ~5% during infilling, producing the same results. Since the material of a crater wall is already disaggragated from the impact event (excluding impact melt that tends to pool in the floor), we believe the volume increase due to erosional disaggradation is likely to be a minor process in crater infilling.

Analyses of the Type E craters indicate that backwasting and enlargement of the crater continued through the terminal stage of degradation. As with the less degraded crater types, the amount of enlargement of the Type E craters appears to have been proportionally greater at larger crater diameters (Table 2). That is, a Type E 20-km-diameter crater must be enlarged by ~15% in order to account for the change in crater depth from infilling by wall material alone, but the amount of enlargement needed increases up to ~31% for a 50-km-diameter crater. In addition to the estimated 5-10 m thick deposit found in the Type B/C craters, another ~55-60 m of material is needed to equilibrate the estimated ~31% enlargement at all Type E crater diameters. It seems plausible that the increase in deposit thickness within Type E craters is due to the lack of a crater rim, which would ordinarily act as a natural topographic barrier. Without the crater rim, infilling from material eroded from the surrounding craters and highlands could have occurred more easily, which implies transport of material over distances of, perhaps, tens of kilometers. An average deposit thickness of 60 m within Type E craters is not unreasonable. Based on the depth to diameter relationship determined for fresh craters in this study (equation (1)), various "ghost" craters in the study area indicate that deposits of material may be >200 m thick in places (e.g., crater centered at -29.0° latitude and 339.4° longitude; Viking orbiter frame 581A55).

Crater Erosion and Rates of Degradation

Having estimated the amount of enlargement and infilling, it is now possible to determine the amount of erosion that may have taken place at any particular crater based on photoclinometric measurements of degradational stage or, alternatively, observed morphology. Although using morphology alone is subject to interpretative errors, it is the only way of estimating the total amount of erosion that may have taken place in the 138 craters that cannot be measured using photoclinometry either because of surface albedo markings or because the image data is otherwise unsuitable for photoclinometry. The only eroded material considered thus far has been the material removed from the crater wall and rim (by backwasting) and deposited in the crater interior (by backwasting and aggradation). However, outer ejecta blankets were also eroded. This volume was estimated algebraically by assuming a flat precrater ground surface, calculating the cross-sectional area from the crater rim crest out to the end of the observable ejecta blanket, and estimating the volume using the Theorem of Pappus (equation (10)). A best fit to these estimates versus crater diameter was made to determine an average exterior (i.e., ejecta blanket) volume. For a fresh crater, the volume of ejecta can be approximated by the equation

$$V_F = 0.007 D_F^{2.931} \tag{11}$$

where V_F is the volume of crater ejecta (km^3) and D_F is the fresh crater diameter (km) defined by the occurrence of maximum rim height.

Eroded interior volume estimates adjusted for aeolian deposition were also plotted against the corresponding degraded crater diameter for each degradation class. The total amount of eroded material can be described by the general equation

$$V_{\text{total}} = V_{\text{int}} + V_{\text{ext}} \tag{12}$$

The interior volume is found to be approximated by

$$V_{\text{int}} = aD_d^b \tag{13}$$

where V_{int} is the volume of eroded material estimated to be within the crater interior (i.e., the area inside the crater rim crest; Figure 6), D_d is the diameter of the observed degraded crater in kilometers, a is the coefficient describing the volume estimated for a crater with a diameter of 1 km, and b is the slope of the of the best fit line (Table 4).

Estimating the volume of material eroded from the crater exterior during degradation is more complicated because it must adjust for the change in crater diameter due to enlargement. Assuming that all craters of a given degradational stage have been enlarged by the calculated amounts (Table 4), the material eroded from the crater exterior can be estimated by

$$V_{\text{ext}} = 0.007[D_d - (D_d c)]^{2.931} - eD_d^f \tag{14}$$

where V_{ext} is the amount of material eroded from the crater exterior through degradation, c is the coefficient describing how much the crater was enlarged at a given stage of degradation, e is the coefficient describing the estimated eroded exterior volume for a 1-km-diameter crater, and f is the slope of the best fit line (Table 4). Note that at a Type E degradational stage the e and f coefficients drop to 0 because the entire ejecta blanket has been

Table 4. Coefficients for Use in Calculating the Volume of Eroded Crater Material (Equations (13) and (14))

Degradational Stage	Interior Coefficients		Enlargement	Exterior Coefficients	
	a	*b*	*c*	*e*	*f*
B/C	0.002	3.174	0.09	0.007	2.623
D	0.003	3.090	0.21	10^{-4}	3.490
E	0.004	3.007	0.31	0.000	0.000

eroded. Essentially, the left-hand of equation (14) describes the volume of exterior ejecta when the crater was fresh, and the right-hand of the equation describes the amount of material still contained as exterior ejecta following degradation.

Estimated Erosion Rates

These equations were applied to all the degraded craters within the study region. The total volume of eroded material for all craters is estimated to be 2.2 x 10^5 km^3, which, if deposited over the entire study area, is equivalent to a layer ~200 m thick. That is not to say that 200 m of material was eroded from the area; it means an equivalent of 200 m of material was reworked and redistributed within the area. This estimate indicates the magnitude of the degradational processes that occurred in the martian highlands. It can also be used as a way of assessing the possible rate at which degradation occurred, but this also requires an assessment of the duration of highland degradation. The time at which degradation ceased can be estimated by the fresh crater population, which, based on the *Tanaka* [1986] model, suggest that degradation ceased in this area during the late Noachian. The onset of degradation is more difficult to determine as it could have occurred anytime prior to the late Noachian. However, two lines of evidence suggest that degradation was not a catastrophic event, but rather a long-lived process that lasted tens to hundreds of millions of years. First, craters observed in this study are preserved at a variety of degradational states at any given size. A short-lived catastrophic event should have eroded all craters at a given diameter the same amount. In addition, our prior work showed that the cessation of degradation was a gradual process that shut-off first at high elevations in the late Noachian and then continued through the early Hesperian at progressively lower elevations [*Craddock and Maxwell,* 1993]. This observation argues against both a short-lived, catastrophic degradational event and, perhaps, multiple, punctuated degradational events as well. In light of these observations, the minimum rate of degradation can be determined by assuming that the onset of this process began when the Npld materials in the study area were emplaced (middle Noachian [*Scott and Tanaka,* 1986]). For comparison, liquid water became stable on Earth at relatively the same time (~4 billion years ago [*Holland,* 1984, p. 110]).

From the *Neukum and Wise* [1976] model chronology, the middle Noachian began ~4.4 Ga and the late Noachian ended ~3.8 Ga. So degradation in this region would have occurred over a 600 million year period [*Tanaka,* 1986]. Alternatively, the *Hartmann et al.* [1981] model places the beginning of the middle Noachian at ~3.92 Ga and the end of the late Noachian at ~3.5 Ga. In their model chronology degradation would have occurred over a 400 million year period [*Tanaka,* 1986]. These intervals suggest that the rate of highland degradation was equivalent to ~0.0003 to 0.0005 mm/yr, respectively, which corresponds to 0.3 to 0.5 Bubnoff units (B). These estimates are equivalent to erosion rates that occur within terrestrial periglacial environments, which range from 0 to 4.0 B and represent the lowest erosion rates on Earth [*Fournier,* 1960].

Craddock and Maxwell [1990, 1993] derived crater size-frequency distribution curves for highland materials over much of the equatorial region of Mars (±30° latitude). These crater curves were then compared to modeled production curves which attempted to accounted for changes in the crater population due to degradation. Essentially, enlargement would shift the cumulative size-frequency distribution to larger crater diameters, and eradication would cause the cumulative number of craters to drop off, especially at smaller diameters. These effects were modeled and incorporated into a production curve that attempted to represent a martian crater population which had not undergone degradation. Subtracting the actual crater size-frequency distribution curves from the modeled ones allowed us to indirectly estimate how much material may have been removed from the martian highlands. The erosion rate estimates made in these studies (0.1-5.0 B [*Craddock and Maxwell,* 1990, 1993]) are also close to estimates derived in this study. These observations support the possibility that the ancient martian environment may have been similar to modern day periglacial environments on Earth, but were the geologic processes that operated on early Mars also similar?

Simulated Mechanisms for Crater Degradation

Which Processes to Model?

There is a great deal of uncertainty concerning the early environment of Mars during the period of crater modification [e.g., *Squyres and Kasting,* 1994]. The widespread occurrence of ancient valley networks and crater modification indicates that weathering, erosion, and deposition occurred more extensively during this time period than later in Mars' history, but the specific processes involved are difficult to determine. For example, some investigators have interpreted the ancient valley networks to have been eroded by surface runoff of liquid water [*Masursky et al.,* 1977], but others have invoked ground water sapping [*Pieri,* 1976, 1980; *Squyres,* 1989]. Estimates of the initial martian water inventory based upon SNC meteorites [*Donahue,* 1995], volcanic outgassing (*R.A. Craddock and R. Greeley,* Estimates of the amount and timing of gases released into the martian atmosphere from volcanic eruptions, submitted to *Meteoritics,*

1997), isotopic data (*B.M. Jakosky and J.H. Jones*, Atmosphere-crust exchange and escape to space, submitted to *Nature*, 1995; hereinafter referred to as submitted paper) and geomorphic features [*Carr*, 1987] range from ~8 to 100's of meters in global depth equivalent. So the major problem is not the supply of water but the difficulty in maintaining atmospheric pressures and temperatures high enough for liquid water to be stable for an extended period of time. Important concerns include atmospheric loss due to impact cratering [*Melosh and Vickery*, 1989], thermal and non-thermal escape of the atmospheric species into space (e.g., *B.M. Jakosky and J.H. Jones*, submitted paper, 1995), and oxidation due to weathering [e.g., *Pollack et al.*, 1987]. Especially problematic is the presumed lower luminosity of the Sun [*Newman and Rood*, 1977; *Gough*, 1981], which requires very high initial atmospheric pressures or perhaps the presence of a greenhouse gas (e.g., methane [*Squyres and Kasting*, 1994]) to maintain a relatively warm early Mars. In addition, even initial pressures of several bars may not be sufficient to maintain a "warm and wet" early Mars because of cloud formation [*Kasting*, 1991]. However, either a somewhat more luminous early Sun [*Whitmire et al.*, 1995], higher orbital obliquities [*Jakosky et al.*, 1995], or the effects of seasonality and heat advection as suggested for the early Earth [*Molnar and Gutowski*, 1995] could possibly allow a periodic martian climate that is marginally above freezing. All of these arguments must be considered when determining a viable set of processes that may have been responsible for martian crater degradation.

Some characteristics of the valley networks themselves and the probable climatic constraints generally argue against widespread, extensive precipitation and runoff. The valley networks have low drainage densities compared to terrestrial drainage basins [*Kochel et al.*, 1985; *Carr*, 1995], they are irregular and patchy in distribution, valley networks are often abruptly terminated, and no channel features or bedforms are visible on the valley bottoms [*Carr*, 1995]. However, because of the very rudimentary dissection involved in the valley networks, only the steepest original slopes (crater walls and ejecta blankets and large regional slopes) would show appreciable incision. Most of the intercrater surface is very low gradient and may be heavily fractured from impact cratering, so that infiltration would have been encouraged over runoff. Furthermore, the valley networks were certainly strongly modified after their formation by mass wasting, which widened and shallowed them [*Goldspiel et al.*, 1993], as well as by aeolian deposition and erosion. Both processes would have obscured or obliterated any primary channel features. Simply, the preserved morphology of the ancient valley networks does not necessarily preclude the possibility of widespread precipitation on early Mars.

Whether the water source is from recharge from below or above, most workers agree that flowing water occupied the valley networks. *Carr* [1995], noting the apparent difficulty in obtaining a "warm and wet" early Mars, and the requirement for 100 to 10^5 times more water flow than net erosional volume during valley erosion [*Howard*, 1988, 1990; *Goldspiel and Squyres*, 1991], suggests that slow mass wasting processes requiring only about as much water as sediment eroded the channels. However, the rheology of sediments argues against this scenario. Most sediment-water mixtures have a finite water content below which intergranular friction prevents motion and above which the flow is fluid-like, but with a finite yield strength. Most debris flows require relatively steep gradients (>10°) to exceed the yield strength, and debris flows are very susceptible to loss of water by evaporation or percolation, causing them to become immobile. Only very fine (clays and colloidal) materials exhibit low yield strength and slow water loss.

Because of the uncertainty of the geochemical, geophysical, and astronomical evidence for the early environment of Mars, we assumed that during crater degradation conditions were suitable for the surface flow of water, possibly ice-covered, resulting either from precipitation or groundwater discharge. This leaves a considerable number of potential scenarios, ranging on one hand from a "normal" hydrologic cycle of precipitation, runoff, and groundwater recharge from above to various mechanisms involving discharge from hydrothermal waters produced either by energy released from crater impacts [*Brakenridge et al.*, 1985], volcanic heat sources [*Wilhelms and Baldwin*, 1989; *Gulick and Baker*, 1990], or added to the near-surface regolith by an "inverted" hydrologic cycle of upward vapor transport from a deep water table [*Clifford*, 1991, 1993; *Moore et al.*, 1995].

Advective and Diffusive Processes

Using the photoclinometrically derived fresh and degraded crater morphometry as a template (Figure 4), we qualitatively explored erosional modification of martian highland craters by a variety of surface processes. The approach taken was two-dimensional where landform development was modeled in cross-section and the rate laws expressed in cylindrical coordinates. Previously, *Howard* [1994] distinguished between advective (scale-efficient) and diffusive (scale-inefficient) erosional processes. Advective processes, such as fluvial erosion and fluvial sediment transport, increase in efficiency with increasing contributing area, so that in steady state erosion (i.e., all parts of the landscape being eroded at the same rate) channel gradient decreases downslope. Conversely, diffusional processes require steeper gradients with increasing contributing area at steady state. Although the martian cratered terrain contains many impact craters that have been modified through degradation, this process was far from having reached a steady state. Nevertheless, the distinction between advective and diffusive processes remains important because advective processes tend to create dendritic channel systems, whereas diffusive processes tend to smooth and round the landscape. Thus, erosion of the valley networks minimally requires a scale-efficient process. Most types of mass-wasting are diffusive, although some high-energy mass wasting such as rockfall and debris avalanches may be advective over short spatial scales. (This is the major difficulty with *Carr's* [1995] suggestion that ancient valley networks were eroded by slow-moving mass wasting flows, in that a scale efficiency must be identified for the proposed mechanism.)

Two-dimensional degradation simulations were used to explore the effects of fluvial erosion and mass wasting on fresh craters. These simulations were based upon the drainage basin evolution model of *Howard* [1994]. One process assumed to modify craters is mass wasting. Potential erosion or deposition due to mass movement of regolith or bedrock, $\partial z/\partial t|_m$, is given by the spatial divergence of the vector rate of movement

$$\left.\frac{\partial z}{\partial t}\right|_m = -K_s \nabla \bullet S \qquad (15)$$

where S is the vector of slope gradient and the constant K_s is assumed to be spatially and temporally invariant. The mass wasting process is diffusive.

Fluvial erosion is advective and can be broken down into two processes: detachment-limited erosion for steep channels flowing on bedrock or regolith in which the bedload sediment flux is less than a capacity load and sediment transport in alluvial channels. The erosion rate in the detachment-limited regime, , $\partial z/\partial t|_c$, is assumed to be proportional to the shear stress, τ, exerted on the bed and banks by the flow

$$\left.\frac{\partial z}{\partial t}\right|_c = -K_t(\tau - \tau_c) \qquad (16)$$

where τ_c is a critical shear stress, which was assumed to be zero in all simulations presented here.

Shear stress can be related to channel gradient and drainage area through the use of equations of steady, uniform flow as discussed by *Howard* [1994], allowing the erosion rate to be re-expressed as a function of contributing area, A, and local channel gradient, S

$$\left.\frac{\partial z}{\partial t}\right|_c = -K_t(K_z A^g S^h - \tau_c) \qquad (17)$$

where K_t and K_z are temporally and spatially invariant, and the exponents g an h have values of 0.3 and 0.7, respectively.

In low-gradient alluvial channels and in depositional areas the potential rate of erosion (or deposition) equals the spatial divergence of the volumetric unit bed sediment transport rate, q_{sb}

$$\left.\frac{\partial z}{\partial t}\right|_c = -\nabla \bullet q_{sb} \qquad (18)$$

Many bedload and total load sediment transport equations for sediment discharge can be expressed as a functional relationship between the two dimensionless parameters, ϕ and $1/\psi$:

$$\phi = K_e\left\{\frac{1}{\psi} - \frac{1}{\psi_c}\right\}^p \qquad (19)$$

where

$$\phi = \frac{q_{sb}}{\omega d (1 - \mu)} \text{ and } \frac{1}{\psi} = \frac{\tau}{(\gamma_s - \gamma) d} \qquad (20)$$

In these equations q_{sb} is the bed sediment transport rate in bulk volume of sediment per unit time per unit channel width, ω is the fall velocity of the sediment grains, d is the sediment grain size, μ is alluvium porosity, and γ_s is the unit weight of sediment grains. As discussed by *Howard* [1994], these equations can be recast into a relationship between total bed sediment discharge, q_{sb}, drainage area, and gradient by assuming a power function relationship between ϕ and $1/\psi$ (equation (20))

$$q_{sb} = K_q A^r [K_v A^s S^t - 1/\psi_c]^p \qquad (21)$$

where K_q and K_v are constants, and the exponents p, r, s and t have values of about 3.0, 0.5, 0.3, and 0.7, respectively.

The simulations assume that the amount of material eroded during an individual erosional event is small compared to the scale of the landform, so that the above processes can be approximated as being continuous. The actual erosion (or deposition) rate at a given point, $\partial z/\partial t$, is a weighted average of the potential mass wasting and fluvial erosion rates [*Howard*, 1994]. These simulations were conducted primarily to explore the effect of crater size on the scaling of creep, weathering, and fluvial erosion and deposition as well as the differences in spatial patterns of erosion and deposition produced by each process. By contrast, scaling of absolute process rates on early Mars is a difficult issue because of uncertainties of physical properties of surface materials and the intensity and duration of erosional processes. Regolith creep diffusivity on Earth ranges from zero to about 0.1 m^2/yr in soils in periglacial environments and some weathered shale.

Figure 7 illustrates the results of these simulations for both 20-km and 40-km-diameter craters. The solid lines indicate the fresh crater morphology from Figure 4 and the dashed lines represent the corresponding crater at the terminal stage of degradation (Type E). In each simulation, the resulting modification was measured over fixed time intervals to assess the process and scale efficiency. If the simulations in Figures 7a and 7b are scaled to K_S of 0.1 m^2/yr (equation (15)), the total simulated time is 75 x 10^6 years. Thus it is conceivable that putative periglacial climates on early Mars could produce modifications of the degree exhibited in Figures 7a and 7b. For this same diffusivity, the maximum weathering rate in Figures 7c and 7d is 4 x 10^{-7} m/yr. Scaling of fluvial erosion is even more difficult because of assumptions that must be made about surface erodibility and frequency and intensity of runoff. However, for the same assumed diffusion scaling, the fluvial erosion rates in Figures 7e and 7g are less than 10^{-6} m/yr, which is a low rate by terrestrial standards.

The simplest process considered was linear diffusional creep (Figures 7a and 7b). This form of creep was assumed to occur at shallow depths relative to the depth of the crater (i.e., a surficial process as opposed to the deeper deformational creep modeled by *Jankowski and Squyres* [1992] for impact crater "softening"). Diffusional creep clearly destroys crater rims and fills in the crater bottoms, producing a profile not unlike the 20-km degraded crater, with the exception of a more bowl-like floor rather than the observed flat floor. However, the same degree of modification of the 40-km crater (Figure 7b) is much less efficient because creep is scale-inefficient, meaning that its efficiency decreases with scale due to longer transport distances.

Linear diffusional creep was locally limited by the further assumption that weathering processes could produce a mobile regolith at a finite rate. This effectively limits the maximum rate of vertical erosion. In locations where the weathering rate

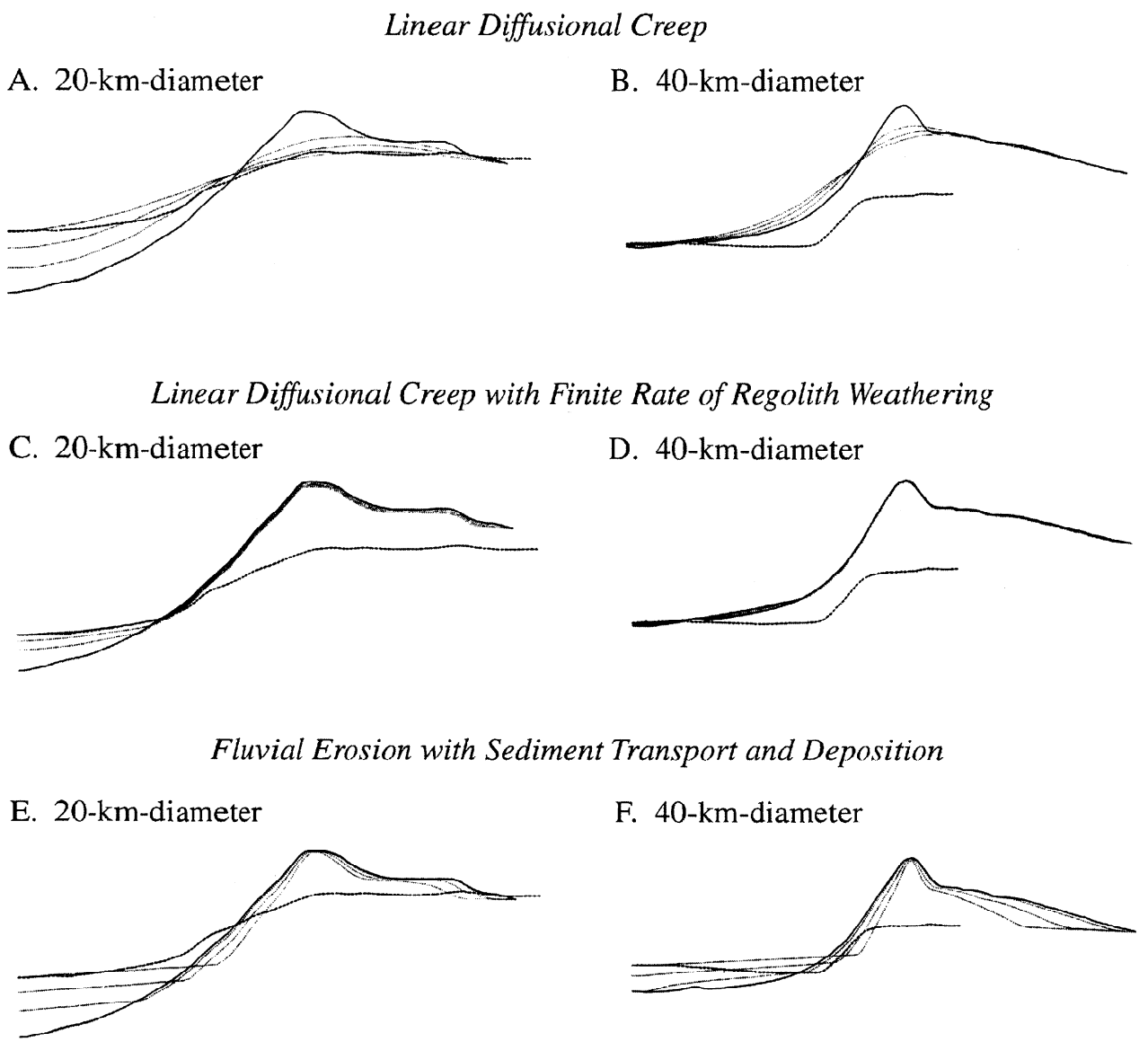

Figure 7. Two-dimensional simulations of possible crater degradation mechanisms. Solid lines indicate the fresh crater morphology, and the dashed lines represent similar diameter craters at the terminal stage of degradation (Figure 4). Note that the degraded crater is not necessarily the endpoint of modification of a fresh crater of the same initial geometry. Dotted lines show subsequent stages of erosional modification. In these simulations the left-hand boundary is free to move vertically but no transported material is allowed to pass through this point (specified zero-flux boundary). The right-hand boundary is fixed at the initial elevation, and mass is conserved in the crater interior but may exit the system at the right boundary. Both 20 and 40 km craters utilize the same rate-governing parameters and total time of simulation. Linear diffusional creep: (a) 20-km-diameter crater; (b) 40-km-diameter crater. This creep is assumed to occur at shallow depths relative to the depth of the crater. In other words, it is modeled as a surficial process as opposed to the deeper deformational creep modeled by *Jankowski and Squyres* [1992] for impact crater "softening." Linear diffusional creep with a finite rate at which mobile regolith can be produced by weathering processes: (c) 20-km-diameter crater; (d) 40-km-diameter crater. Fluvial erosion and sediment transport and deposition: (e) 20-km-diameter crater; (f) 40-km-diameter crater. (g) and (h) Similar to Figures 7e and 7f except that a fixed standing water level is assumed. Combination of fluvial erosion-deposition and diffusional creep: (i) 20-km-diameter crater; (j) 40-km-diameter crater.

became limiting, it was assumed that slopes were weathering- rather than transport-limited. The combination of creep and weathering-limiting erosion (Figures 7c and 7d) is ineffective at reducing crater rims (at least for the uniform weathering rate assumed), but crater floors are infilled, forming an abrupt break in slope and a fairly flat crater floor. This combination of processes is also scale inefficient and is much less capable of producing similar modification of larger craters.

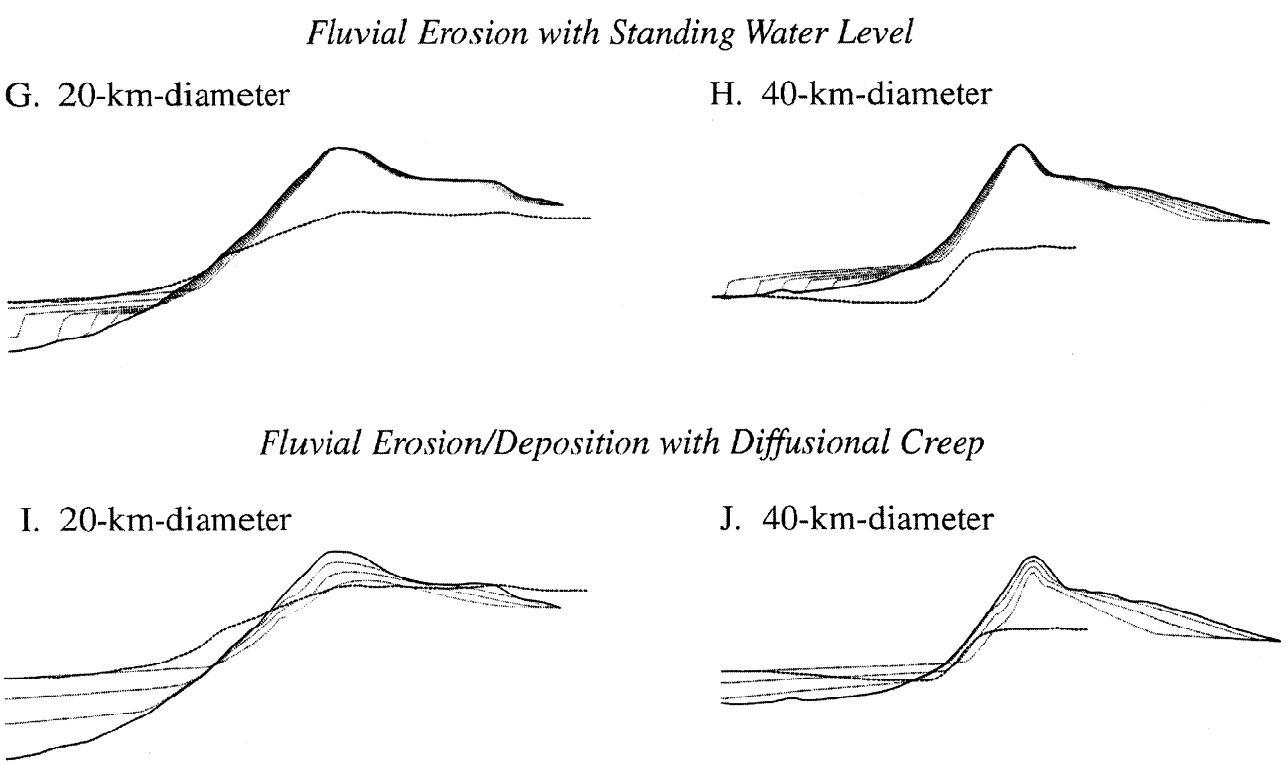

Figure 7. (continued)

Fluvial erosion at a rate proportional to the shear stress was also considered while permitting sediment transport and deposition. Sediment transport and erosional detachment were parameterized as a function of local surface gradient and contributing area as discussed by *Howard* [1994]. Fluvial erosion is scale-efficient in that more rapid erosion occurs for larger contributing areas for the same gradient. This results in approximately the same relative modification for both the 20- and 40-km-diameter craters (Figures 7e and 7f). The steeper crater walls are predicted to be bedrock channels whose erosion is limited by the rate of detachment. The crater floors and some portions of the ejecta blanket are sediment-covered, and generally are aggradational. In addition, because of the dependency of erosion rate on contributing area, erosion of crater rims is slight and erosion of the outer rim and lower crater wall is rapid, steepening the slope gradients. Thus, in contradistinction to creep, water erosion by itself appears incapable of reducing crater rims and lowering overall wall rim gradients.

Fluvial erosion and deposition were also simulated with a fixed standing water level (Figures 7g and 7h), so that fluvial deposition would involve progradation of a deltaic form. Although not observed in the study area, this process is capable of producing an inner crater terrace similar to those described by *Forsythe and Zimbelman* [1995] in the Memnonia region and attributed to fluvial deposition.

The simulation closest to producing equivalent degrees of modification (i.e., enlargement, infilling and erosion) at both large and small diameter craters involved a combination of fluvial erosion and deposition with diffusional creep. Figures 7i and 7j illustrates the effect of combining scale-efficient and scale-inefficient processes.

This cursory analysis illustrates the usefulness of this approach in determining the processes and combination of processes that could be responsible for highland crater degradation. A variety of constraints and processes were not considered in these simulations, including spatially variable resistance of the crater materials to weathering, detachment and transport, the occurrence of rapid mass wasting on steep slopes due to rock or regolith failure, and sapping erosion by flowing water. The combination of creep and fluvial erosion seems to be unable to explain the large amount of crater enlargement that occurred during degradation as inferred by the morphometric analysis. This is because the raised rim acts as a drainage divide for both creep and fluvial erosion. A groundwater sapping process may be much more effective in producing crater enlargement, because groundwater from the plains beyond the rim can contribute to erosion of the crater wall. Future simulations will address this problem.

Conclusions

1. Our observations of fresh craters support the results of *Pike and Davis* [1984]. Although a much larger sample of fresh martian impact craters was analyzed using the *Davis and Soderblom* [1984] photoclinometric model, the morphometric relations between rim height and depth to crater diameter were very similar to those determined by *Pike and Davis* [1984]. However, our observations do suggest that the crater rim height is much more variable than prior results indicate.

2. Photoclinometric measurements of degraded impact craters provide the first quantitative descriptions of the highland crater degradation sequence. During the initial stages of degradation (Type B/C craters), crater central peaks were quickly removed.

Crater rims were also downcut and the interior slopes became shallower. Continued degradation eventually removed the crater rims completely, infilled the crater interiors to produce a broad, flat floor, and dramatically decreased the average interior slope (Type D and E craters). The observed crater modifications are not supportive of depositional processes exclusively. Rather, they are indicative of a predominately erosional process(es).

3. The simple algebraic model presented here, which balanced the mass eroded from the crater sides with the measured amount of infilled material, indicates that backwasting increased crater diameters by ~10% initially and by as much as 30% by the terminal stage of degradation. Assuming backwasting is a scale-efficient process, the relative amounts of crater enlargement should be equal at any crater diameter. In order for the calculated enlargement percentage to be equal at any given Type B/C diameter crater, a deposit ~10 m thick had to infill these craters following the degradational process. Because the presence of a crater rim, albeit eroded, precludes the likelihood of additional material being transported overland into the crater interior, it is presumed that this deposit is aeolian in origin. Alternatively, ~5% volume expansion of eroded materials occurred. Similarly, craters at the terminal stage of degradation (Type E) must contain a deposit ~60 m thick to explain the calculated difference in crater enlargement at different diameters. Because these craters lack a rim, material eroded from the exteriors of surrounding features could have infilled these craters. This suggests that at least some of the material eroded from the highlands was transported lateral distances of tens of kilometers or, in other words, that there was extensive overland transport of sediments due to degradation.

4. The morphometric relations derived from photoclinometric measurements allowed us to develop equations that describe the volume of material eroded from a crater of a given diameter at any stage of degradation. Within the study area, we calculated that ~2.2 x 10^5 km^3 of material was eroded, suggesting that an equivalent of ~200 m of material was reworked and redistributed in the Margaritifer Sinus/Sinus Sabaeus region. Depending on which model chronology is used, degradational processes may have been active for approximately 400 or 600 million years. These estimates correspond to an erosion rate of ~0.0003 to 0.0004 mm/yr, which is equivalent to those experienced in terrestrial periglacial environments [*Fournier*, 1960]. This implies that the early martian climate may have been similar.

5. Two-dimensional simulations of linear diffusional creep and fluvial erosion and deposition suggest that fluvial erosion alone is incapable of producing the observed crater morphology. A combination of both of these processes produces modified craters with similar observed morphologies. These preliminary results indicate the usefulness of this approach. Accurate determination of the mechanism(s) responsible for highland crater modification will have to wait until a larger population of craters is analyzed and wider variety of processes is modeled. However, these preliminary results argue that early Mars experienced widespread precipitation, fluvial processes, and near surface groundwater flow.

Future Work

Ideally, the shape of a fresh crater at a given diameter could be described by some n-th order polynomial equation. The shape of a degraded crater at any stage of degradation could also be described by an nth order polynomial; however, the corresponding diameter would have to be adjusted for a given amount of enlargement due to backwasting. Determining the amount of material eroded by backwasting versus the amount of material deposited into the crater interior becomes a simple matter of integrating the two equations, determining the corresponding volumes by solids of revolution, and adjusting the degraded crater diameter until both the eroded and infilled volumes balance and the remaining change in crater depth is approximated. The problem we encountered, however, was deriving a polynomial equation that accurately described a crater at a given diameter and encompassed the observed least squares morphometry. A measured 20-km-diameter fresh crater, for example, might have the same crater depth described by equation (1) yet possess a rim height that was too high or too low to be described by equation (2). Currently, this is a function of the small crater population analyzed in this study. Future work will concentrate on refining the morphometric relations presented here, establishing the applicability of these relations to other geologic materials in the southern highlands, determining variations in the intensity and duration of degradation within the highlands, and simulating probable processes that may have operated in the early history of Mars.

Appendix: Photoclinometry

Photoclinometry is a technique for obtaining topographic data from a single, monoscopic image. This method is based on the principle that variations in brightness values measured by an imaging system are directly related to the orientation of the surface element relative to both the sun and the camera. However, there are several additional sources that cause variations in brightness. An important source for non-topographic brightness variations within an image comes from the detector itself. Specifically, the vidicon system on board the Viking orbiters had a nonuniform response across the field of view due to variations in the electric field and the angle of the electron beam to the photoconductor surface [*U.S. Geological Survey*, 1987, Section 3.1, p. 16]. The result is an image that appears "shaded." In addition, the photoconductors always measure a low-level energy signature that is a function of temperature, scan rate, light-flood conditions, gain state, and offset condition. Known as a dark current, this effect is the result of the electric charge that builds up in the electronics when there are no photons hitting the conductors. Fortunately, however, the Viking Visual Imaging Subsystem is well-calibrated and these brightness variations, which are typically <12%, can be removed. Prior to flight the Viking vidicons were calibrated using a light cannon with a known spectral radiance [*Klaasen et al.*, 1977]. Further, the vidicons were also evaluated inflight for performance and changes [*Thorpe*, 1976; *Klaasen et al.*, 1977; *U.S. Geological Survey*, 1987]. These data provide radiometric corrections that are applied to an image during processing prior to making photoclinometric measurements.

Additional spacecraft sources of brightness variations that affect photometric analyses include coherent and random noise from the cameras as well as noise introduced into the images by telemetry problems. Such inherent noises typically affect only

relatively small portions of individual images and are easily identified. The coherent noise generally occurs at the top and bottom of the Viking frames and thus the overlap between images is usually such that the affected areas can be trimmed. Craters examined in this study affected by coherent noise in one frame were often visible in another. Because reseau marks do not contain any photometric information, we also avoided taking photoclinometric profiles across these artifacts.

An important external source for non-topographic brightness variations within an image is scattering in the martian atmosphere [see discussion by *Davis and Soderblom*, 1984]. Atmospheric scattering causes a certain percentage of solar radiation to be reflected directly off the atmosphere and into the spacecraft camera before falling incident onto the surface. Solar radiation can also be reflected from the atmosphere directly onto the surface and then into the spacecraft camera, but the contribution from this effect is proportionally less due to surface absorption, which is a function of the surface albedo. The light scattered into the camera by these various mechanisms is collectively referred to as additive scattering effects. Similarly, light can be scattered away from the camera producing subtractive scattering effects. As described below, these effects can be removed in the photoclinometric model developed by *Davis and Soderblom* [1984].

A final source of brightness variations that is particularly problematic for photoclinometry on Mars is surface albedo variation. Craters on Mars are especially susceptible to albedo variations because they act as aeolian barriers and traps that induce windstreak formation and deposition of intracrater materials [*Arvidson*, 1974a; *Greeley et al.*, 1974; *Veverka et al.*, 1981; *Lee*, 1984; *Thomas*, 1984; *Presley and Arvidson*, 1988; *Greeley et al.*, 1992]. Typically we avoided measuring craters with associated windstreaks. We also observed that in certain craters brightness levels between the crater interior and surrounding highlands differed from ~3 to 20 DN within a dynamic range of 0 to 10,000 (i.e., the default 16-bit dynamic range); however, variations of >40 DN were sometimes observed. Craters with such large differences in brightness values from the surrounding highlands were also avoided because of our interpretation that a significant portion of this brightness was due to non-topographic effects. Because of albedo variations, the resulting number of analyzed craters is not the inclusive crater population within the study area. A total of 138 degraded craters and >200 fresh craters contained within the study area were excluded from the photoclinometric analysis primarily due to extreme variations in surface albedo.

The procedure for deriving a photoclinometric profile begins by updating the labels to the selected raw Viking Orbiter image (PICS-SPICELAB), locating and zeroing-out reseaus, and applying the radiometric corrections (PICS-RADCAL). The operator then displays the image and determines a haze factor from an average low DN measured in a shadow typically within a large crater. Care must be used in evaluating a shadowed surface because radiation scattered from surface element to surface element can cause overestimation of the true DN due to atmospheric scattering [*Davis and Soderblom*, 1984; *Tanaka and Davis*, 1988]. In some cases, we also observed that the haze values sometimes varied significantly within a given frame so multiple measurements were sometimes necessary. The measured DN value of shadows is entered into the program to provide a correction for additive atmospheric scattering. To correct for subtractive scattering effects, the operator chooses a starting point at the geometric center of a crater and two end points outside the crater rim. Preferably, the end points will be in opposing directions but parallel to the direction of illumination (sun azimuth). The assumption made in choosing the photoclinometric profiles is that the albedo and topography are radially symmetric about the crater. Brightness values along both profiles are ratioed to each other pixel by pixel from the crater center outwards. The result is an expression that is a function of the surface normal orientation or the Minnaert photometric equation:

$$B=B_0 \cos^k i \cos^{k-1} e \qquad (22)$$

where B_0 is the surface normal albedo, i is the solar incidence angle, and e is the emission angle [*Minnaert*, 1941]. The Minnaert coefficient, k, is a function of wavelength and varies directly with phase angle. Viking orbiter red filter images are similar in spectral response to Mariner 9 Television Experiment images [*Thorpe*, 1976], so the values of k calculated by *Thorpe* [1973] using Mariner data were applied. *Tanaka and Davis* [1988] have also developed values of k for the Viking Orbiter clear and minus-blue filters.

Acknowledgments. This research has benefited from useful discussions with Bruce Campbell, John Grant, Jim Head, and Jim Zimbelman. Special thanks to Frank Chuang for his tireless effort in supporting this work. R.A.C. is especially grateful to Mark Robinson for his patience in explaining the intricacies of the photoclinometric module in PICS and for Tom Watters' support. Nadine Barlow and Jules Goldspiel provided very constructive reviews of this manuscript. This research is supported by NASA grants NAGW- 3920 (Smithsonian Institution) and NAGW- 1926 (University of Virginia).

References

Arvidson, R.E., Windblown streaks, splotches, and assorted craters on Mars: Statistical analysis of Mariner 9 photographs, *Icarus, 21*, 12-27, 1974a.

Arvidson, R.E., Morphologic classification of Martian craters and some implications, *Icarus, 22*, 264-271, 1974b.

Arvidson, R.E., M. Coradini, A. Carusi, A. Coradini, M. Fulchignoni, C. Federico, R. Funiciello, and M. Salomone, Latitudinal variation of wind erosion of crater ejecta deposits on Mars, *Icarus, 27*, 503-516, 1976.

Arvidson, R.E., K.A. Goettel, and C.M. Hohenberg, A post-Viking view of martian geologic evolution, *Rev. Geophys., 18*, 565-603, 1980.

Barlow, N.G., Quantifying crater degradation in Maja Valles and Memnonia, Mars (abstract), *Lunar Planet. Sci., XXIII*, 63-64, 1992.

Barlow, N.G., Increased depth-diameter ratios in the Medusae Fossae formation deposits of Mars (abstract), *Lunar Planet. Sci., XXIV*, 61-62, 1993.

Barlow, N.G., The degradation of impact craters in Maja Valles and Arabia, Mars, *J. Geophys. Res., 100*, 23,307-23,316, 1995.

Barlow, N.G., and T.L. Bradley, Martian impact craters: Correlations of ejecta and interior morphologies with diameter, latitude, and terrain, *Icarus, 87*, 156-179, 1990.

Brakenridge, G.R., H.E. Newsom, and V.R. Baker, Ancient hot springs on Mars: Origins and paleoenvironmental significance of small Martian valleys, *Geology, 13*, 859-862, 1985.

Carr, M.H., Water on Mars, *Nature, 326*, 30-35. 1987.

Carr, M.H., The martian drainage system and the origin of valley networks and fretted channels, *J. Geophys. Res., 100*, 7479-7507, 1995.

Carr, M.H., and G.D. Clow, Martian channels and valleys: Their characteristics, distribution, and age, *Icarus, 48*, 91-117, 1981.

Chapman, C.R., Cratering on Mars, I. Cratering and obliteration history, *Icarus, 22*, 272-291, 1974.

Chapman, C.R., and K.L. Jones, Cratering and obliteration history of Mars, *Annu. Rev. Earth Planet. Sci., 5*, 515-540, 1977.

Clifford, S.M., Role of thermal vapor diffusion in the subsurface hydrologic evolution of Mars, *Geophys. Res. Lett., 18*, 2055-2058, 1991.

Clifford, S.M., A model for the hydrologic and climatic behavior of water on Mars, *J. Geophys. Res., 98*, 10,973-11,016, 1993.

Craddock, R.A., and F. Chuang, The Mechanisms for forming martian rampart craters: Clues from crater morphometry (abstract), *Lunar Planet. Sci., XXVII*, 263-264, 1996.

Craddock, R.A., and T.A. Maxwell, Resurfacing of the martian highlands in the Amenthes and Tyrrhena region, *J. Geophys. Res., 95*, 14,265-14,278, 1990.

Craddock, R.A., and T.A. Maxwell, Geomorphic evolution of the martian highlands through ancient fluvial process, *J. Geophys. Res., 98*, 3453-3468, 1993.

Davis, P.A., and L.A. Soderblom, Modelling crater topography and albedo from monoscopic Viking orbiter images, *J. Geophys. Res., 89*, 9449-9457, 1984.

DeHon, R.A., Thickness of ridged plains materials in Hesperia Planum, Mars (abstract), *Lunar Planet. Sci., XVI*, 173-174, 1985.

Donahue, T.M., Evolution of water reservoirs on Mars from D/H ratios in the atmosphere and crust, *Nature, 374*, 432-434, 1995.

Forsythe, R.D., and J.R. Zimbelman, A case for ancient evaporite basins on Mars, *J. Geophys. Res., 100*, 5553-5563, 1995.

Fournier, F., *Climat et Erosion: la Relation Entre l'Erosion du Sol par l'Eau et les Precipitations Atmospheriques*, 201 pp., P.U.F., Paris, 1960.

Goldspiel, J.M., and S.W. Squyres, Ancient aqueous sedimentation on Mars, *Icarus, 89*, 392-410, 1991.

Goldspiel, J.M., S.W. Squyres, and D.G. Jankowski, Topography of small martian valleys, *Icarus, 105*, 479-500, 1993.

Gough, D.O., Solar interior structure and luminosity variations, *Solar Phys., 74*, 21-34, 1981.

Grant, J.A., and P.H. Schultz, Gradational epochs on Mars: Evidence from west-northwest of Isidis basin and Electris, *Icarus, 84*, 166-195, 1990.

Grant, J.A., and P.H. Schultz, The gradational history of southern Ismenius Lacus (abstract), *Lunar Planet. Sci., XXII*, 485-486, 1991a.

Grant, J.A., and P.H. Schultz, Styles of crater degradation in southern Ismenius Lacus, Mars (abstract), *Lunar Planet. Sci., XXII*, 487-488, 1991b.

Grant, J.A., and P.H. Schultz, Degradation of selected terrestrial and Martian impact craters, *J. Geophys. Res., 98*, 11,025-11,042, 1993.

Grant, J.A., and P.H. Schultz, Early fluvial degradation in Terra Terrain, Mars: Constraints from styles of crater degradation on the Earth (abstract), *Lunar Planet. Sci., XXV*, 457-458, 1994.

Greeley, R., and J.E. Guest, Geologic map of the eastern hemisphere of Mars, scale 1:15M, *U.S. Geol. Surv. Misc. Invest. Ser. Map, I-1802-B*, 1987.

Greeley, R., J.D. Iversen, J.B. Pollack, N. Udovich, and B. White, Wind tunnel simulations of light and dark streaks on Mars, *Science, 183*, 847-849, 1974.

Greeley, R., N. Lancaster, S. Lee, and P. Thomas, Martian aeolian processes, sediments, and features, in *Mars*, edited by H.H. Kieffer, B.M. Jakosky, C.W. Snyder, and M.S. Matthews, pp. 730-766, Univ. of Ariz. Press, Tucson, 1992.

Gulick, V.C., and V.R. Baker, Origin and evolution of valleys on Martian volcanoes, *J. Geophys. Res., 95*, 14,325-14,344, 1990.

Hartmann, W.K., Martian cratering, III, Theory of crater obliteration, *Icarus, 15*, 410-428, 1971.

Hartmann, W.K., et al., Chronology of planetary volcanism by comparative studies of planetary cratering, in *Basaltic Volcanism on the Terrestrial Planets*, pp. 1049-1127, Pergamon, Tarrytown, New York, 1981.

Holland, H.D., *The Chemical Evolution of the Atmosphere and Oceans*, 582 pp., Princeton Univ. Press, Princeton, N.J., 1984.

Howard, A.D., Introduction: Groundwater sapping on Mars and Earth., in *Sapping Features of the Colorado Plateau*, edited by A.D. Howard, R.C. Kochel, and H. Holt, *NASA Spec. Pub. 491*, pp. 1-5, 1988.

Howard, A.D., Groundwater and fluvial erosion on Mars: Recharge or dewatering? (abstract), Rep. Planet. Geol. Geophys. Prog., *NASA Tech. Memo., 4210*, 345-347, 1990.

Howard, A.D., A detachment-limited model of drainage basin evolution, *Water Resourc. Res., 30*, 2261-2285, 1994.

Jakosky, B.M., B.G. Henderson, and M.T. Mellon, Chaotic obliquity and the nature of the Martian climate, *J. Geophys. Res., 100*, 1579-1584, 1995.

Jankowski, D.G., and S.W. Squyres, The topography of impact craters in "softened" terrain on Mars, *Icarus, 100*, 26-39, 1992.

Jones, K.L., Evidence for and episode of crater obliteration intermediate in martian history, *J. Geophys. Res., 79*, 3917-3931, 1974.

Kasting, J.F., CO_2 condensation and the climate of early Mars, *Icarus, 94*, 1-13, 1991.

Klaasen, K.P., T.E. Thorpe, and L.A. Morobito, Inflight performance of the Viking Visual Imaging system, *Appl. Optics, 16*, 3158-3170, 1977.

Kochel, R.C., A.D. Howard, and C.F. McLane, Channel networks developed by groundwater sapping in fine-grained sediments: Analogs to some martian valleys, in *Models in Geomorphology*, edited by M.J. Woldenberg, pp. 313-341, Allen and Unwin, Winchester, Mass., 1985.

Lee, S.W., Mars: Wind streak production as related to obstacle type and size, *Icarus, 58*, 339-357, 1984.

Leighton, R.B., B.C. Murray, R.P. Sharp, J.D. Allen, and R.K. Sloan, Mariner IV photography of Mars: Initial results, *Science, 149*, 627-630, 1965.

Masursky, H., J.M. Boyce, A.L. Dial, G.G. Schaber, and M.E. Strobell, Classification and time formation of Martian channels based on Viking data, *J. Geophys. Res., 82*, 4016-4038, 1977.

Maxwell, T.A., and R.A. Craddock, Age relations of Martian highland drainage basins, *J. Geophys. Res., 100*, 11,765-11,780, 1995.

McGill, G.E., and D.U. Wise, Regional variations in degradation and density of Martian craters, *J. Geophys. Res., 77*, 2433-2441, 1972.

Melosh, H.J., and A.M. Vickery, Impact erosion of the primordial martian atmosphere, *Nature, 338*, 487-489, 1989.

Minnaert, M., The reciprocity principle in lunar photometry, *Astrophys. J., 93*, 403-410, 1941.

Molnar, G.I., and W.J. Gutowski, The "faint young Sun paradox"; further exploration of the role of dynamical heat-flux feedback in maintaining global climate stability, *J. Glaciol., 41* (137), 87-90, 1995.

Moore, J.M., Nature of mantling deposit in the heavily cratered terrain of northeastern Arabia, Mars, *J. Geophys. Res., 95*, 14,279-14,289, 1990.

Moore, J.M., G.D. Clow, W.L. Davis, V.C. Gulick, D.R. Janke, C.P. McKay, C.R. Stoker, and A.P. Zent, The circum-Chryse region as a possible example of a hydrologic cycle on Mars: Geologic observations and theoretical evaluation, *J. Geophys. Res., 100*, 5433-5448, 1995.

Mouginis-Mark, P., Martian fluidized crater morphology: Variations with crater size, latitude, altitude, and target material, *J. Geophys. Res., 84*, 8011-8022, 1979.

Neukum, G., and D.U. Wise, Mars: A standard crater curve and possible new time scale, *Science, 194*, 1381-1387, 1976.

Newman, M.J., and R.T. Rood, Implications of solar evolution for the Earth's early atmosphere, *Science, 198*, 1035-1037, 1977.

Oliver, H.J., A new engineering: Geological rock durability classification, *Eng. Geol.*, 14, 255-279, 1979.

Pieri, D., Distribution of small channels on the Martian surface, *Icarus, 27*, 25-50, 1976.

Pieri, D., Martian valleys: Morphology, distribution, age, and origin, *Science, 210*, 895-897, 1980.

Pike, R.J., and P.A., Davis, Toward a topographic model of Martian

craters from photoclinometry (abstract), *Lunar Planet. Sci., XV*, 645-646, 1984.

Pollack, J.B., J.F. Kasting, S.M. Richardson, and K. Poliakoff, The case for a wet, warm climate on early Mars, *Icarus, 71*, 203-224, 1987.

Presley, M.A., and R.E. Arvidson, Nature and origin of materials exposed in the Oxia Palus-Western Arabia-Sinus Meridiani region, Mars, *Icarus, 75*, 499-517, 1988.

Scott, D.H., and K.L. Tanaka, Geologic map of the western hemisphere of Mars, scale 1:15M, *U.S. Geol. Surv. Misc. Invest. Map, I-1802-A*, 1986.

Soderblom, L.A., T.J. Kreidler, and H. Masursky, Latitudinal distribution of a debris mantle on the Martian surface, *J. Geophys. Res., 78*, 4117-4122, 1973.

Squyres, S.W., Urey Prize lecture: Water on Mars, *Icarus, 79*, 229-288, 1989.

Squyres, S.W., and M.H. Carr, Geomorphic evidence for the distribution of ground ice on Mars, *Science, 231*, 249-252, 1986.

Squyres, S.W., and J.F. Kasting, Early Mars: How warm and how wet?, *Science, 265*, 744-749, 1994.

Tanaka, K.L., The stratigraphy of Mars, *Proc. Lunar Planet. Sci. Conf. 17th*, Part 1, *J. Geophys. Res., 91*, suppl., E139-E158, 1986.

Tanaka, K.L., and P.A. Davis, Tectonic history of the Syria Planum province of Mars, *J. Geophys. Res., 93*, 14,893-14,907, 1988.

Thomas, P.C., Martian intracrater splotches: Occurrence, morphology, and colors, *Icarus, 57*, 205-227, 1984.

Thorpe, T.E., Mariner 9 photometric observations of Mars from November 1971 through March 1972, *Icarus, 20*, 482-489, 1973.

Thorpe, T.E., The Viking Orbiter camera's potential for photometric measurement, *Icarus, 27*, 229-239, 1976.

U.S. Geological Survey, *Planetary Image Cartography System Users Manual*, Flagstaff, Ariz., 1987.

Veverka, J., P. Gierasch, and P. Thomas, Wind streaks on Mars: Meteorological control of occurrence and mode of formation, *Icarus, 45*, 154-166, 1981.

Whitmire, D.P., L.R. Doyle, R.T. Reynolds, and J.J. Matese, A slightly more massive young Sun as an explanation for warm temperatures on early Mars, *J. Geophys. Res., 100*, 5457-5464, 1995.

Wilhelms, D.E., and R.J. Baldwin, The role of igneous sills in shaping the martian uplands, *Proc. Lunar Planet. Sci., 19th*, 355-365, 1989.

R.A. Craddock and T.A. Maxwell, Center for Earth and Planetary Studies, Room 3776, National Air and Space Museum, MRC-315, Smithsonian Institution, Washington, D.C. 20560, USA. (e-mail: craddock@ceps.nasm.edu)

A.D. Howard, Department of Environmental Sciences, University of Virginia, Charlottesville, Virginia 22903.

(Received June 24, 1996; revised April 3, 1997;
accepted April 11, 1997.)